CORRECTED 1 MAY 2019; SEE ERRATUM

TISSUE ENGINEERING

Bioengineered human acellular vessels recellularize and evolve into living blood vessels after human implantation

Robert D. Kirkton[1], Maribel Santiago-Maysonet[1], Jeffrey H. Lawson[1,2], William E. Tente[1], Shannon L. M. Dahl[1], Laura E. Niklason[1,3], Heather L. Prichard[1]*

Traditional vascular grafts constructed from synthetic polymers or cadaveric human or animal tissues support the clinical need for readily available blood vessels, but often come with associated risks. Histopathological evaluation of these materials has shown adverse host cellular reactions and/or mechanical degradation due to insufficient or inappropriate matrix remodeling. We developed an investigational bioengineered human acellular vessel (HAV), which is currently being studied as a hemodialysis conduit in patients with end-stage renal disease. In rare cases, small samples of HAV were recovered during routine surgical interventions and used to examine the temporal and spatial pattern of the host cell response to the HAV after implantation, from 16 to 200 weeks. We observed a substantial influx of alpha smooth muscle actin (αSMA)–expressing cells into the HAV that progressively matured and circumferentially aligned in the HAV wall. These cells were supported by microvasculature initially formed by $CD34^+/CD31^+$ cells in the neoadventitia and later maintained by $CD34^-/CD31^+$ endothelial cells in the media and lumen of the HAV. $Nestin^+$ progenitor cells differentiated into either $αSMA^+$ or $CD31^+$ cells and may contribute to early recellularization and self-repair of the HAV. A mesenchymal stem cell–like $CD90^+$ progenitor cell population increased in number with duration of implantation. Our results suggest that host myogenic, endothelial, and progenitor cell repopulation of HAVs transforms these previously acellular vessels into functional multilayered living tissues that maintain blood transport and exhibit self-healing after cannulation injury, effectively rendering these vessels like the patient's own blood vessel.

INTRODUCTION

The clinical demand for safe and effective vascular repair material is substantial. Cardiovascular disease, including disorders that require the bypassing of occluded or narrowed blood vessels, remains the leading cause of patient morbidity and mortality in the world (*1*). The repair and reconstruction of congenital cardiovascular defects and vessels disrupted during traumatic injury, oncologic surgery, or organ transplantation, as well as the creation of arteriovenous (AV) conduits for hemodialysis access, often require the use of vascular substitutes. Autologous arteries and veins are typically the primary choice of material for vascular repair or creation of AV fistulas; however, the option for harvesting and repurposing vessels within the same patient is often limited by the pathophysiological condition of the patient. Consequently, synthetic vascular grafts and patches such as those constructed from expanded polytetrafluorethylene (ePTFE) or polyethylene terephthalate (Dacron) have been implanted in millions of patients over the past four decades, but their use comes with higher risks of infection, thrombosis, and other complications compared to the use of autologous arteries or veins (*2*, *3*).

Numerous biological alternatives to autologous vessels and synthetic vascular grafts, including both allogeneic and xenogeneic vessels and tissues, have been evaluated and approved by the U.S. Food and Drug Administration for human implantation. However, their potential is limited by availability, cost, processing techniques, and mixed clinical outcomes (*4*). Specifically, the methods used to cryopreserve, fix, sterilize, or decellularize allogeneic and xenogeneic tissues often affect their immunogenicity and biocompatibility, resulting in host inflammatory reactions, and ultimately, in material degradation and mechanical failure (*5*–*8*). Although many of these tissues have mechanical strengths that match or exceed those of native autologous vascular tissue, the structure and composition of their matrix are not conducive for appropriate repopulation by host cells (*9*–*11*). Thus, these allogeneic and/or xenogeneic tissues are never sufficiently remodeled into the host's own living tissue. Identifying when and what types of host cells participate in the repopulation and remodeling of implanted vascular material becomes critical for understanding their long-term success or failure in patients.

With continued clinical evaluation and development of scalable and cost-efficient manufacturing processes, readily available tissue-engineered human blood vessels may offer a promising "off-the-shelf" and biocompatible alternative to allogeneic, xenogeneic, and synthetic vascular grafts (*4*). Advances in tissue engineering have established a promising new paradigm in regenerative medicine in which biological tissues are generated in vitro with the goal of recapitulating the structure and function of their native equivalents in vivo. Approaches for tissue-engineered blood vessels have progressed substantially in 30 years since they were first conceived (*12*), and to date, several designs have been evaluated in a variety of human cardiovascular applications including repair of congenital heart defects (*13*–*15*), hepatic portal vein bypass (*16*), and most recently, AV conduits for hemodialysis access in patients with kidney failure (*17*, *18*).

We have developed an investigational bioengineered blood vessel, the human acellular vessel (HAV), that is generated by seeding human vascular cells into a biodegradable mesh scaffold within a bioreactor system. This system provides pulsatile distention, culture medium circulation, and allows for decellularization of the resulting collagenous blood vessel (to remove all cells and immunogenic

[1]Humacyte Inc., Durham, NC 27713, USA. [2]Departments of Surgery and Pathology, Duke University Medical Center, Durham, NC 27710, USA. [3]Departments of Anesthesiology and Biomedical Engineering, Yale University, New Haven, CT 06511, USA. *Corresponding author. Email: prichard@humacyte.com

potential) while retaining the mechanical integrity of its extracellular matrix (*19*, *20*). To date, these HAVs have been implanted in over 240 patients with end-stage renal failure requiring hemodialysis access during two phase 2 (*17*) and two on-going phase 3 clinical trials. Over 444,000 people suffering from end-stage renal disease (ESRD) use chronic hemodialysis for renal replacement therapy in the United States alone (*21*). Because access for hemodialysis is associated with frequent complications requiring surgical revisions, this clinical setting provides a unique opportunity for histopathological evaluation of small tissue segments that are explanted during routine surgical interventions. In this study, we systematically evaluated explanted HAV specimens from our phase 2 clinical trial patients, with implant durations ranging from 16 to 200 weeks to produce a comprehensive analysis of human clinical remodeling of an engineered vascular tissue.

RESULTS

Generation and characterization of HAVs

Bioengineered HAVs measuring 35 to 42 cm long with an inner diameter of 6 mm were produced in custom bioreactors for clinical implantation, using pulsatile circulation with cyclic radial strain followed by decellularization. Structural and mechanical characterization of these HAVs yielded an average cross-sectional wall thickness of 440 ± 85 μm (n = 97), suture strength of 210 ± 53 g (n = 109), and burst pressure of 2914 ± 928 mmHg (n = 5) (*17*). These mechanical attributes were similar to, or exceeded those of, native human internal mammary artery (*22*) and saphenous vein (*22*, *23*). The ultrastructure of the decellularized HAV extracellular matrix (ECM) was analyzed at multiple positions using scanning electron microscopy (SEM) (Fig. 1A). The outer abluminal surface (Fig. 1B) and inner luminal surface (Fig. 1C) have a dense fibrillar network of ECM. Sectioning the HAV in the transverse (Fig. 1D) or longitudinal (Fig. 1E) plane revealed that, throughout the sectioned wall of the HAV, the ECM fibers were circumferentially aligned.

HAV clinical implantation, hemodialysis access, and retrieval of explanted samples

Sixty patients (20 in the United States and 40 in Poland) with end-stage renal failure were each implanted with an HAV for use as an AV graft during two phase 2 clinical trials conducted within the United States and Poland (*17*). Each HAV was implanted within the upper arm, connecting the brachial or axillary artery to the brachial or axillary vein (Fig. 2A). Blood flow rate and HAV diameter were measured using ultrasound to confirm patency (Fig. 2B). Follow-up ultrasonography of HAVs from 15 days to 1 year after implantation showed a slight decrease in the mean blood flow rate and a slight increase in HAV mean diameter; however, these differences were not statistically significant as determined by one-way analysis of variance (ANOVA) and post hoc Tukey's multiple comparisons tests (Fig. 2C). The slight decrease in flow rate was expected and is commonly seen in AV conduits due to narrowing of the venous outflow tract after AV connection. Cannulation of the HAVs for hemodialysis, typically three times per week, was commenced 4 to 8 weeks after implantation (Fig. 2D). One year after implantation, the primary, primary-assisted, and secondary patency rates for the HAVs in the 60 patients were 28, 38, and 89%, respectively.

Thirteen of the 60 patients had routine AV interventions to address either thrombosis or pseudoaneurysm due to cannulation trauma that resulted in surgical revision and explant of HAV segments, at times spanning 16 to 200 weeks after implantation (table S1). Three of the 13 patients had HAV samples explanted at two different time points, which resulted in a total of 16 tissue explants retrieved and processed for histological analysis. Although all samples received were stained and evaluated, we focused on four representative samples chosen at chronologically distributed time points (16, 55, 100, and 200 weeks after implantation) for presentation and discussion. However, representative staining images from all 16 explanted samples, as well as additional cell characterization studies, are also provided (figs. S1 to S10).

Temporal evaluation of cell infiltration and matrix remodeling by H&E and trichrome staining

Routine hematoxylin and eosin (H&E) staining of HAV cross sections before implantation and at numerous times after implantation (Fig. 3 and fig. S1) showed that the HAV became repopulated with host cells, primarily but not exclusively from the abluminal surface. A distinct neoadventitial layer containing microvessels was identifiable even at the shortest implant duration time point (16 weeks, Fig. 3C). The HAV progressively became more recellularized by host cells over time, with further development of the medial and neoadventitial layers and perivascular integration with surrounding adipose and epithelial tissues (Fig. 3, G and I). The dense ECM of the HAV, consisting primarily of collagen (Fig. 3, B, D, F, H, and J), was maintained throughout implantation in the samples examined.

Immunohistochemical evaluation of host immune and inflammatory cells in HAV explants

Fluorescence immunostaining revealed that the majority of the infiltrating host cells throughout all explant time points appeared to be nonimmune and noninflammatory cells. Specifically, few $CD3^+$ T cells and few to no $CD20^+$ B cells were

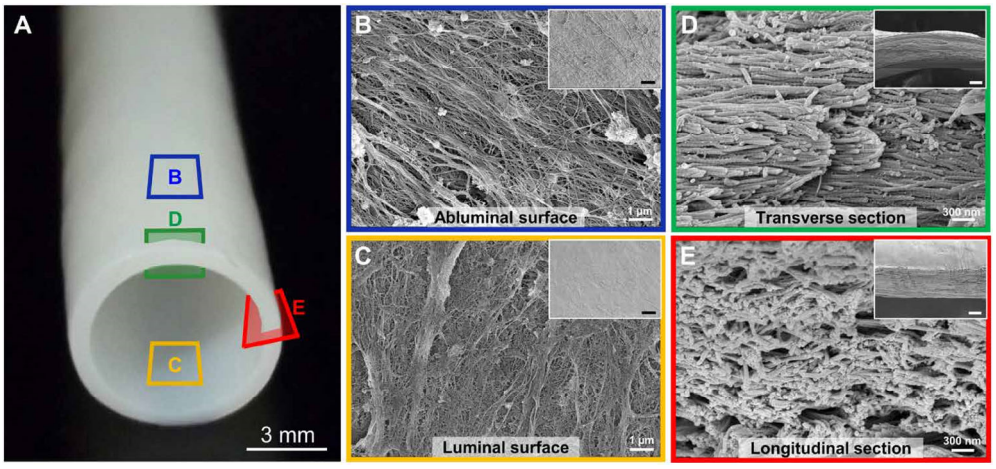

Fig. 1. Ultrastructure of the HAV matrix. (**A**) Image of a bioengineered HAV (6-mm inner diameter) depicting sections taken for SEM to examine matrix architecture. (**B**) Outer and (**C**) inner surface SEMs. (**D**) Transverse and (**E**) longitudinal within-wall cross-sectional SEMs. Lower magnification is shown in insets. Scale bars, 60 μm (B and C) or 150 μm (D and E).

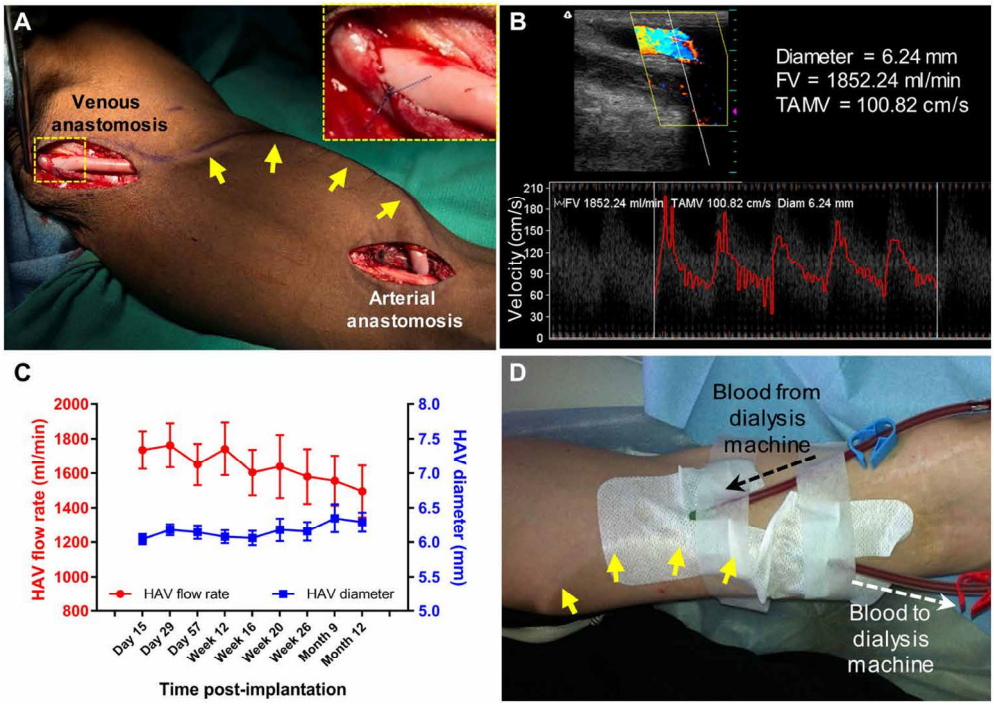

Fig. 2. Clinical HAV implantation and hemodialysis access. (**A**) Intraoperative image of HAV implantation in the upper arm of a patient with end-stage renal failure for use as an AV conduit. The HAV was tunneled under the skin (yellow arrows) and connected the axillary vein at the venous anastomosis (inset) to the brachial artery (arterial anastomosis). (**B** and **C**) Postoperative Doppler ultrasound measurements of mid-HAV diameter, blood flow volume (FV), and time averaged mean velocity (TAMV) during follow-up within the patient population. Data are shown as means ± SE (n = 28 to 59 HAVs) with no significant differences (P > 0.05) as determined by ANOVA and post hoc multiple comparisons tests. (**D**) Photograph of cannulation of the subdermal HAV (yellow arrows) for hemodialysis. Cannulation was performed multiple times a week to patients starting at 4 or 8 weeks after implantation. Images courtesy of S. Rocko at Duke University Medical Center (A) and J. Turek at Wroclaw Medical University (D).

found dispersed in all retrieved explant samples (fig. S2). We also immunostained all HAV explants and control tissue sections (human tonsil) for the presence of classically activated (proinflammatory) M1 and alternatively activated (anti-inflammatory) M2 host macrophages using the subtype-specific markers CD80 and CD206, respectively (*24*, *25*). The staining revealed a few sparse $CD80^+$ proinflammatory M1 macrophages in 3 of the 16 HAV explants (fig. S3). $CD206^+$ anti-inflammatory M2 macrophages were identified in all HAV explants, with earlier explant time points (fig. S3, A to J) showing relatively higher concentrations of $CD206^+$ cells compared to later explant time points (fig. S3, K to P). The overall concentration of these $CD206^+$ cells was low compared to the total number of 4′,6-diamidino-2-phenylindole (DAPI)–labeled cells within the explanted HAV samples. Coexpression of the pan-macrophage marker CD68 was observed in both $CD80^+$ and $CD206^+$ cells; however, some $CD68^+$ cells lacked CD80 or CD206 expression. Human tonsil control tissue sections had an abundance of both $CD80^+$ and $CD206^+$ cells that coexpressed CD68 (fig. S3, Q to T).

Repopulation and evolution of host smooth muscle actin–positive cells within the implanted HAV

Immunofluorescence staining for alpha smooth muscle actin (αSMA) revealed αSMA^+ cells surrounding neoadventitial microvessels and within the medial layer of the HAV (Fig. 4 and fig. S4). The αSMA^+ cells, likely smooth muscle cells (SMCs) or myofibroblasts, progressively increased in density within the medial layer over time, became more elongated and circumferentially aligned, and increased coexpression of the mature contractile SMC marker calponin 1 (CNN1) with time of implant duration (Fig. 4 and fig. S4). Some of the αSMA^+ cells surrounding larger microvessels also coexpressed CNN1.

Angiogenic vascularization and luminal endothelialization of the implanted HAV

$CD34^+$ cells, typically considered either hematopoietic (*26*) or endothelial (*27*) progenitor cells, were detected among the dense population of neoadventitial microvessels within the earliest explant at 16 weeks after implantation (Fig. 5A). These $CD34^+$ cells also expressed the ubiquitous endothelial marker, CD31 [platelet endothelial cell adhesion molecule-1 (PECAM-1)]; however, in larger microvessels, $CD31^+$ endothelial cells lacked CD34 expression (Fig. 5B, white arrow), implying loss of progenitor phenotype. With increased implantation time, neovascularization progressed into the medial layer, and the total $CD34^+$ cell population declined (Fig. 5 and fig. S5). $CD31^+$ expression remained consistent with microvessels in the medial layer, increasing in size and density with time of implantation. Perfused transverse and longitudinal medial microvessels were observed in the later HAV explant time points (Fig. 5H).

Nearly complete luminal coverage by $CD31^+$ endothelial cells was found within a mid-vessel section of an HAV that was patent 44 weeks after implantation (Fig. 5I). The 44-week explant was unique among the 16 retrieved explants in that this HAV had never had a prior intravascular surgical intervention and was fully patent at the time of partial resection due to a cannulation site pseudoaneurysm. Thus, this sample provided a rare opportunity to evaluate endothelialization in an undisturbed HAV implant. This sample was explanted from the middle of the HAV, the most distant point from potential transanastomotic migration of native host endothelial cells, suggesting that luminal coverage by endothelial cells was established mid-HAV within 44 weeks after implantation. These luminal cells were also positive for both CD144 (vascular endothelial-cadherin or VE-cadherin) and endothelial nitric oxide synthase (eNOS), indicative of a mature and functional endothelial lining on the HAV lumen (Fig. 5, J to L).

Infiltration and differentiation of $Nestin^+$ progenitor cells

Nestin, an intermediate filament protein originally described in neural stem cells and embryonic tissues, has been shown to be expressed in developing and regenerating vasculature (*28*). At 16 weeks after implantation, we identified a dense population of Nestin-expressing cells localized in a circumferential band within the neoadventitia (Fig. 6A and fig. S6A). At later explant time points (18 to 55 weeks

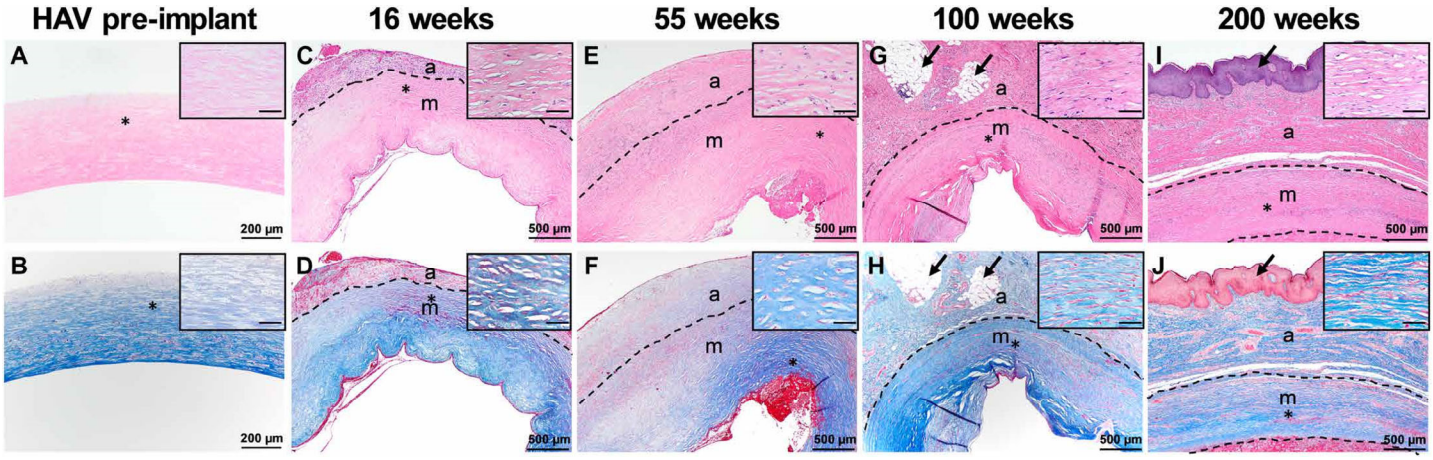

Fig. 3. Representative routine staining of HAVs before and after implantation. (**A** and **B**) H&E staining of HAV before implantation shows acellular matrix stained pink without purple nuclei, whereas Masson's trichrome reveals blue-stained collagen fibers (B). (**C** to **J**) Stained samples explanted 16 (C and D), 55 (E and F), 100 (G and H), and 200 (I and J) weeks after implantation. a, neoadventitia; m, medial layer; border delineated by a black dashed line. Integration of the HAV neoadventitia with perivascular adipose (G and H, black arrows) and epithelial (I and J, black arrow) tissue. HAV explant sections were taken from mid-graft (16 and 200 weeks) or venous anastomosis (55 and 100 weeks) regions. Insets: Higher magnification of medial layer area denoted by "*". Scale bars, 50 μm (insets).

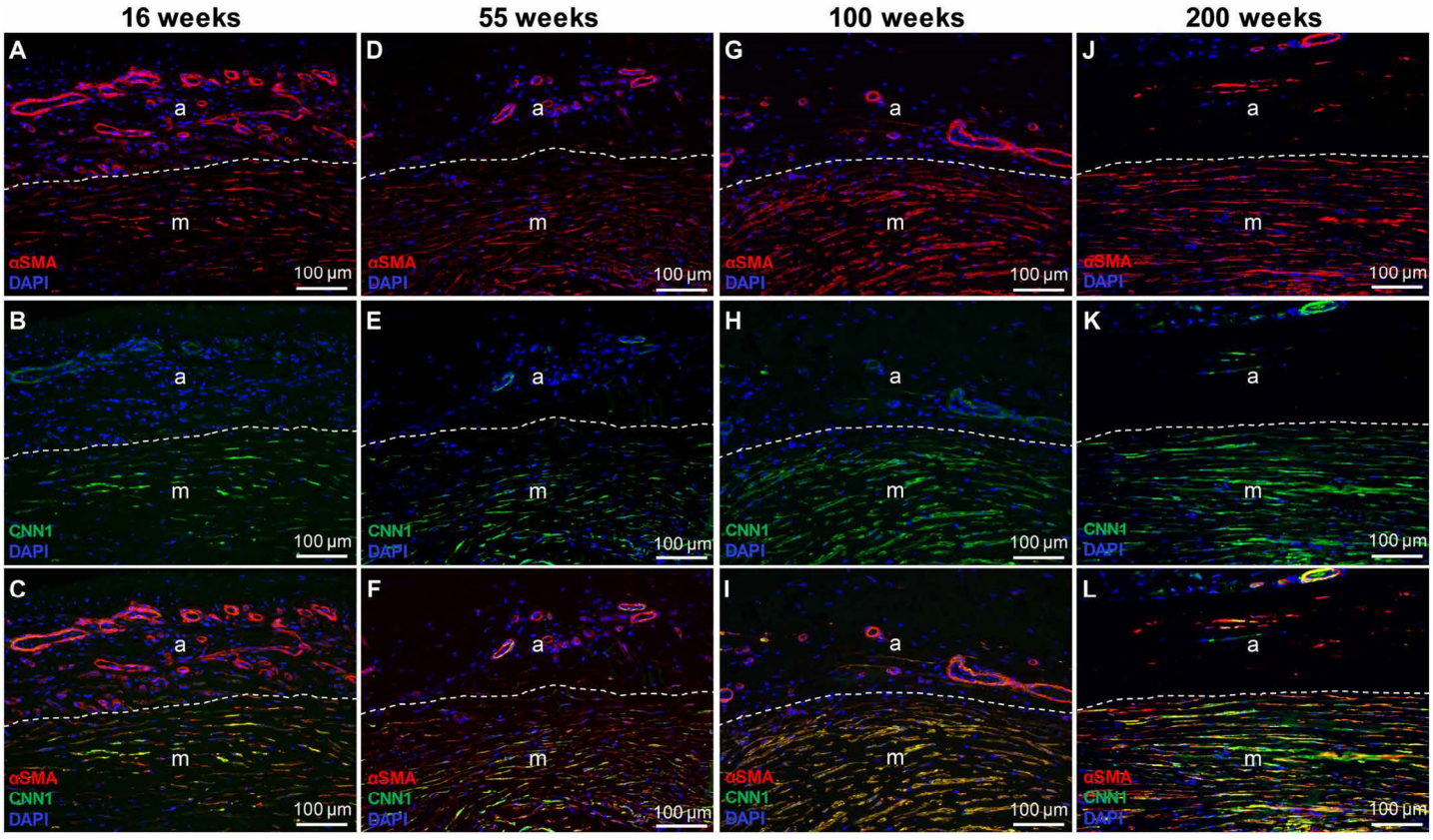

Fig. 4. Infiltration and maturation of αSMA$^+$ host cells within the implanted HAV. Immunofluorescence staining of explanted HAV sections for αSMA (red) and CNN1 (green), a contractile marker of mature SMCs. Developmental maturation indicated by coexpression of CNN1 and αSMA. HAV sections explanted at 16 (**A** to **C**), 55 (**D** to **F**), 100 (**G** to **I**), and 200 (**J** to **L**) weeks after implantation. a, neoadventitia; m, medial layer. The boundary between the neoadventitia and medial layers is delineated by a white dashed line. Nuclei (blue) were counterstained with DAPI.

after implantation), most Nestin$^+$ cells were localized within the medial layer and were less numerous (Fig. 6B and fig. S6, B to J). Only a few Nestin$^+$ cells were dispersed in the medial layer within explants isolated more than 55 weeks after implantation (fig. S6, K to P, and Fig. 6, C and D). Staining at 16 weeks suggested that Nestin$^+$ cells were capable of transitioning into myogenic or endothelial cell types, based on colocalization of Nestin with αSMA (Fig. 6, E to H) or CD31 (Fig. 6, I to L), respectively. We observed Nestin$^+$/αSMA$^+$ and

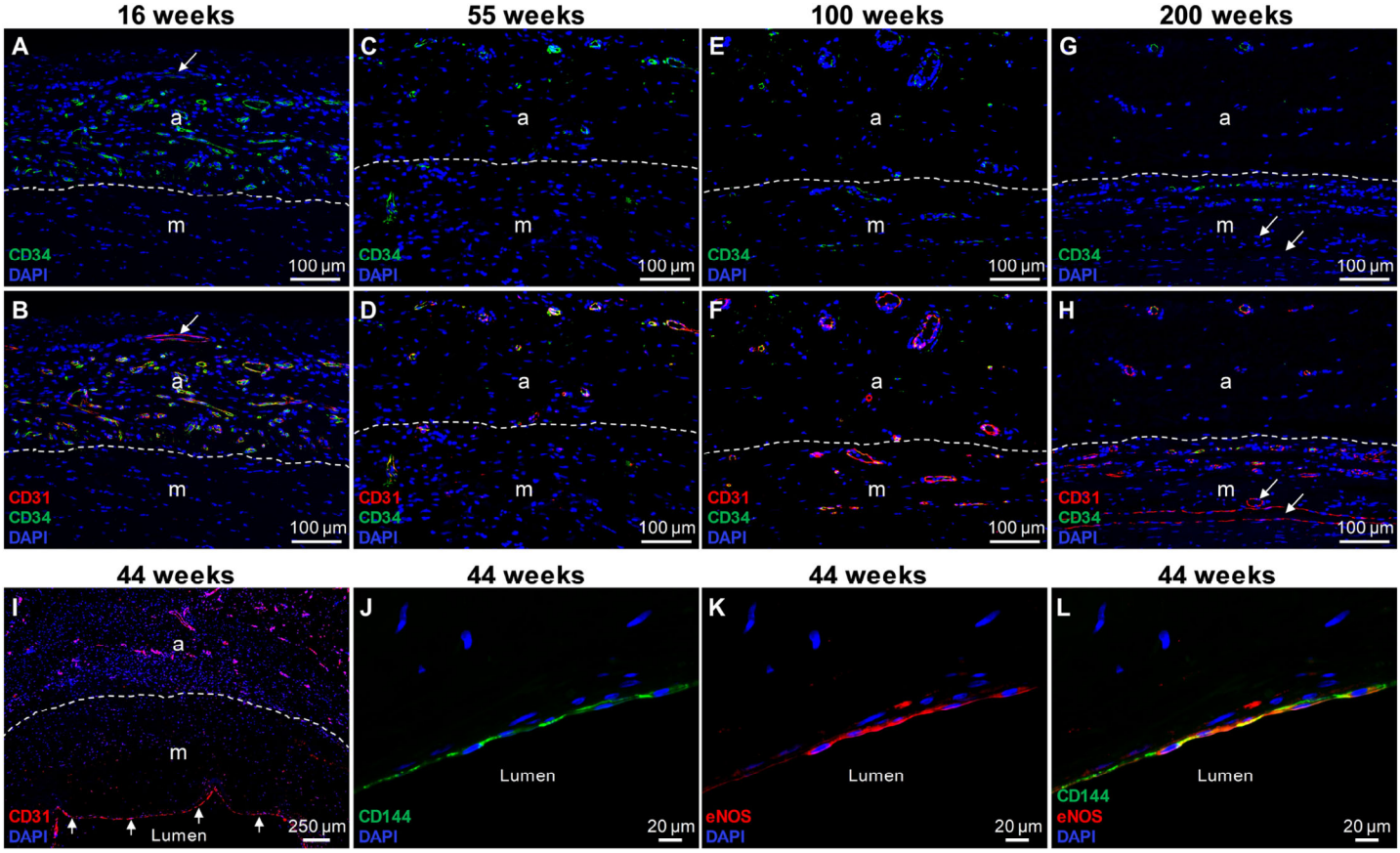

Fig. 5. Angiogenic vascularization and luminal endothelialization of the implanted HAV. (**A**) Immunofluorescence staining for the endothelial progenitor marker CD34 revealed numerous angiogenic CD34$^+$ cells (stained green) forming microvessels within the neoadventitia (a) at 16 weeks after implantation. (**B**) CD34$^+$ cells co-expressed the ubiquitous endothelial marker CD31 (red), but CD31$^+$ cells in some larger microvessels lacked CD34 expression (A and B, white arrows). HAV sections explanted at 55 (**C** and **D**), 100 (**E** and **F**), and 200 (**G** and **H**) weeks after implantation. White arrows in (G) and (H) highlight microvessels with CD34$^-$/CD31$^+$ cells. (**I**) CD31$^+$ endothelial cells (red) lining both the lumen and microvessels of a mid-HAV explant at 44 weeks after implantation. (**J** to **L**) Luminal cells express VE-cadherin (CD144, green) and eNOS (red). a, neoadventitia; m, medial layer; a white dashed line was drawn to delineate neoadventitia and medial layers (A to I). Nuclei (blue) were counterstained with DAPI.

Nestin$^+$/CD31$^+$ cells, as well as cells expressing solely Nestin, αSMA, or CD31 (without colocalization). However, we did not find any αSMA$^+$/CD31$^+$ cells of "indeterminant" commitment to smooth muscle versus endothelial fate (fig. S7). Thus, the Nestin$^+$/αSMA$^+$ and Nestin$^+$/CD31$^+$ cell populations appear to be distinct and may both arise from an earlier Nestin$^+$ precursor, although this is speculative.

αSMA$^+$/Nestin$^+$ cells identified in regions of HAV self-repair after cannulation injury

Masson's trichrome staining of a mid-HAV segment explanted after 44 weeks revealed two areas of cannulation-related injury to the HAV wall that appeared to be in the process of healing (fig. S8, A to C). Histology showed a dense population of host cells within a collagenous matrix in these regions of repair. Most cells within these regions expressed αSMA, with some of these cells also expressing Nestin (fig. S8, D to F).

Progressive accumulation of MSC-like CD90$^+$ cells in the HAV

Immunofluorescence costaining for αSMA and CD90 identified small, round αSMA$^-$ cells with strong CD90 expression that progressively increased in number with duration of HAV implantation (Fig. 7, A to D, and fig. S9). None of these cells were found in the 16-week sample, whereas the percentage of CD90$^+$ cells increased significantly ($P < 0.05$) at each subsequent explant time point (0.8 ± 0.5%, 3.5 ± 0.9%, 8 ± 3% CD90$^+$ cells/mm^2 in the 55-, 100-, and 200-week samples, respectively; Fig. 7E). Although most of these αSMA$^-$/CD90$^+$ cells were dispersed in the neoadventitia, they were also present within the medial layer of the HAV explants starting 55 weeks after implantation. In addition to not expressing αSMA, the CD90$^+$-expressing cells did not express CD34 (Fig. 5F), CD45 (leukocyte common antigen; Fig. 5G), endothelial markers CD31 and CD144, nor the pericyte marker CD13 (fig. S10, A to C). However, the CD90$^+$ cells did co-express CD44 and CD73 (Fig. 5, H and I), as well as CD140a (platelet-derived growth factor receptor α; fig. S10D), making them consistent with mesenchymal stem or stromal cells (MSCs).

DISCUSSION

Previous histopathological analyses of explanted vascular grafts have demonstrated that the host cell response often determines the fate of the implanted material. Commercially available synthetic grafts can provoke inflammatory reactions, fail to integrate properly into the surrounding tissue, and can inhibit host neutrophil behavior leading

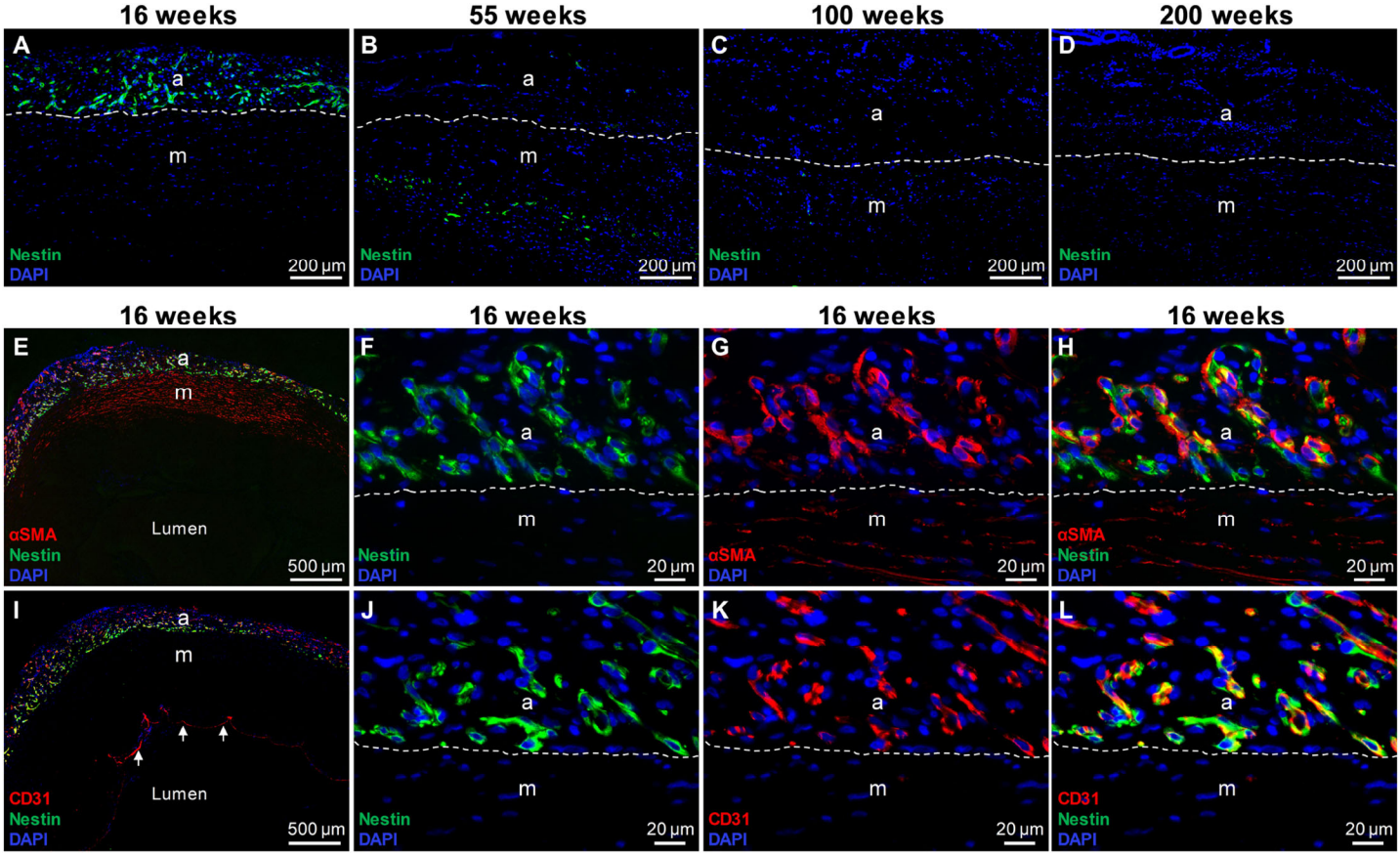

Fig. 6. Migration and differentiation of Nestin$^+$progenitor cells within the implanted HAV. (**A** to **D**) Immunofluorescence staining for the intermediate filament Nestin (green) within HAVs explanted at 16 (A), 55 (B), 100 (C), and 200 (D) weeks after implantation. (**E** to **L**) Sixteen-week HAV explant samples immunostained for expression of Nestin (green) and αSMA (red) (E to H) or Nestin (green) and CD31 (I to L). Coexpression indicated by overlay of combined staining (yellow) (H and L). CD31$^+$ cells were found (white arrows) on lumen of 16-week HAV explant (I). a, neoadventitia; m, medial layer; a white dashed line was drawn to delineate neoadventitia and medial layers. Nuclei (blue) were counterstained with DAPI.

to sustained bacterial infections (*29*–*31*). Chemically cross-linked, sterilized, or cryopreserved allografts and xenografts have also been shown to trigger inflammatory and immune responses and fail to appropriately recellularize (*32*–*35*). In contrast, the preimplant HAVs are completely decellularized and mechanically robust with circumferentially aligned ECM, but are not chemically cross-linked and have no synthetic components. We have previously shown promising but limited histological evidence that the HAV is favorably repopulated by host cells in preclinical (*19*) and clinical (*17*) studies.

In this study, we performed the most extensive histological and immunofluorescence evaluation of an engineered human tissue to date. Hemodialysis access is a clinical setting that often requires interventions and surgical revisions of the conduit in response to hemodynamic- and cannulation-induced complications. Thus, it provides a unique opportunity to acquire implanted tissue for histological examination of host remodeling over a long time period, up to 4 years in this study. At the earliest time point, 16 weeks after implantation, we observed a substantial amount of recellularization, primarily from the surrounding connective tissue but also from some cells infiltrating into the HAV from the circulation. Stratification of the HAV into neoadventitial and medial layers was already beginning at this time, and a large number of microvessels were present within the neoadventitial layer.

Most of the cells dispersed within the media of the HAV at 16 weeks were αSMA$^+$ and thus were likely either SMCs or myofibroblasts. Immunofluorescence costaining of the 16-week explant for both αSMA$^+$ and the mature SMC marker, calponin (CNN1) (*36*), revealed that many of the αSMA$^+$ cells within the medial layer and around some larger microvessels were expressing a contractile phenotype. At extended durations of implantation, the medial layer of the HAV consisted of a dense population of circumferentially aligned αSMA$^+$/CNN1$^+$ cells. In addition to SMCs, the HAV explants were also evaluated for the presence of immunological and inflammatory cells that might signal an adaptive or innate immune response. On the basis of the relatively small number of dispersed CD3$^+$ T cells and even fewer CD20$^+$ B cells and CD80$^+$ proinflammatory M1 macrophages detected, it appears that the HAV did not elicit substantial immune responses in any of the patients from which the explanted tissues were retrieved and analyzed. This is consistent with previously reported immunohistochemistry and serum analysis in the patient population (*17*).

Angiogenic neovascularization of the HAV was well established in the neoadventitia at the 16-week time point. This process was driven by cells expressing CD34, a transmembrane glycoprotein that is critical during embryonic vasculogenesis (de novo blood vessel formation) (*37*) and is expressed in both hematopoietic (*26*) and

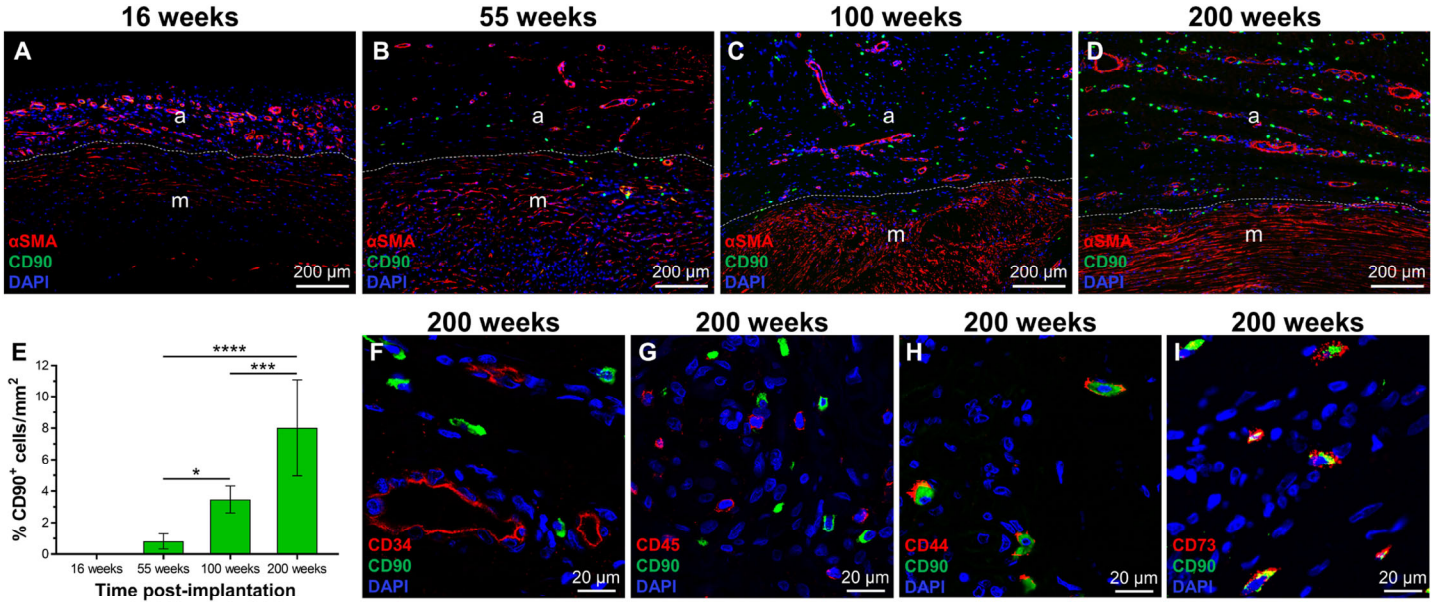

Fig. 7. Progressive influx of MSC-like host cells within the implanted HAV. (**A** to **D**) Immunofluorescence staining of HAV explants for αSMA and CD90 at indicated time points after implantation. (**E**) Quantification of $CD90^+$ cells/mm^2. Immunofluorescence staining of 200-week HAV explants for CD90 (green) and (**F**) CD34 (red), (**G**) CD45 (red), (**H**) CD44 (red), and (**I**) CD73 (red) expression. a, neoadventitia; m, medial layer; a white dashed line was drawn to delineate neoadventitia and medial layers in (A) to (D). Nuclei (blue) were counterstained with DAPI. For (E), eight random images were taken from each explant section, and the percentage of cells (DAPI, blue) that expressed CD90 (green) was calculated per area imaged. Data are shown as means ± SD with statistical differences of $^*P < 0.05$, $^{***}P < 0.0005$, and $^{****}P < 0.0001$ as determined by ANOVA and post hoc multiple comparisons tests.

endothelial (*27*) progenitor cells. Expression of CD34 decreased with time of implantation and with increasing size of microvessels. In contrast, CD31 (PECAM-1) expression in these cells remained relatively constant over time. These results are consistent with previous in vivo and in vitro studies showing that CD34 expression is predominantly localized to actively angiogenic cells in small capillaries (*38*). Moreover, during the maturation of the neoadventitial microvasculature, we observed a reduction of the microvessel density, perhaps comparable to the process of vascular pruning that occurs during remodeling of neovascularized beds (*39*).

Surgical interventions and balloon-assisted thrombectomy can cause denudation of luminal endothelium, and some explant samples did not contain an intact luminal endothelium. However, we identified $CD31^+$ luminal endothelial cells in the 16-week explant (Fig. 6I), and more complete coverage in a mid-vessel section of an HAV never subjected to intravascular interventions and patent when explanted at 44 weeks (Fig. 5I). These luminal cells also expressed VE-cadherin (CD144) and eNOS (Fig. 5L), implying barrier and anticoagulant function. These results provide ongoing evidence that luminal repopulation of HAVs is possible, either from circulating progenitors or from direct cellular in-growth from neighboring tissues. Although further studies would be needed to investigate the modes of HAV endothelialization, preclinical studies from Pennel *et al.* (*40*, *41*), using modified ePTFE loop grafts with porous polyurethane inserts, demonstrated three potential mechanisms of graft endothelialization that include transanastomotic outgrowth, transmural capillary ingrowth from perivascular tissue, and fallout endothelialization from circulating cells. This group also performed histological examination of long-term clinical explants from patients implanted with in vitro endothelialized ePTFE femoropopliteal bypass grafts, which revealed substantial in vivo formation of pannus-like tissue in between the graft and endothelial layer (*42*). Contrary to our observations in HAV explants, this tissue contained dense populations of inflammatory cells including lymphocytes, macrophages, and foreign body giant cells. Regions of aligned αSMA^+ cells, within the intraluminal tissue but not the ePTFE graft, were also identified, suggesting the possibility of either endothelial cell transdifferentiation or colonization by circulating myogenic progenitor cells.

Beyond the vascular phenotypes, we observed two distinct progenitor populations during HAV remodeling in humans. One cell population expressed Nestin, an intermediate filament found in neural stem cells (*43*), skeletal myoblasts (*44*), and endothelial cells (*45*) during embryonic development. The finding of $Nestin^+$ cells in conjunction with the $CD34^+$ cell population during early HAV recellularization may suggest that the remodeling process has some resemblance to embryonic vasculogenesis. It is possible that a combination of SMC-derived ECM proteins in the HAV, along with cyclic mechanical cues provided by the arterial circulation, drives the recruitment and differentiation of these embryonic-like vascular progenitors. $Nestin^+$ cells appeared first in the neoadventitia adjacent to the medial layer within the 16-week explant; subsequent explants revealed $Nestin^+$ cells primarily in the medial layer. However, there was less overall Nestin expression with increasing duration of implantation.

Costaining in early explants revealed that $Nestin^+$ cells were capable of transitioning into myogenic or endothelial cell types based on colocalization with αSMA or CD31, respectively. Nestin coexpression with αSMA (*46*, *47*) or CD31 (*46*, *48*) was observed previously in neonatal and postnatal blood vessels within animal models. In adult animal and human tissues, populations of $Nestin^+$ cells have also been identified, but it is believed that they typically remain quiescent until reactivated. Nestin expression in pulmonary (*49*) and

cardiac (*50*) fibroblasts has been shown to increase proliferation and activation of these cells during reactive and reparative fibrosis. In addition, Nestin$^+$ cells have also been shown to facilitate tissue repair (*28*), including regeneration of injured skeletal (*51*), cardiac (*52*), and vascular smooth (*47*) muscle. In this study, we observed that Nestin$^+$/αSMA$^+$ cells appeared to be actively repairing cannulation injuries in the HAV wall. This process appeared to be mainly confined to repopulation and regeneration of the lost HAV matrix and may also suggest that Nestin expression may decrease as the repaired tissue matures.

In contrast to CD34$^+$ and Nestin$^+$ progenitor cells, which decreased in number during increasing duration of HAV implantation, CD90$^+$ cells substantially increased over time. Although these cells primarily reside within the neoadventitia, they were also occasionally found dispersed in the medial layer. Immunofluorescence staining characterized these cells as CD90$^+$, CD44$^+$, CD73$^+$, and CD140a$^+$ but CD13$^-$, CD31$^-$, CD34$^-$, CD45$^-$, CD144$^-$, and αSMA$^-$. MSCs are known to express CD90, CD44, CD73, and CD140a but not CD31, CD34, CD45, and CD144 (*53*–*55*). Therefore, these cells appear to be MSC-like. However, differences between MSC phenotypes identified in various tissues and time points, as well as whether the cells are examined in situ or in vitro, make classification and comparison of MSC cell surface markers challenging (*53*).

The speculation that various stem and progenitor cell populations reside within perivascular or vascular wall niches (*56*, *57*), including a subadventitial vasculogenic zone (*58*), is being actively pursued (*59*). Although we show that Nestin$^+$ progenitor cells can coexpress CD31 or αSMA, the role and fate of the progressively accumulating CD90$^+$ MSC-like cell population and whether these cells are establishing a stem cell niche around the HAV remain unclear. Because these cells do not express CD34 or CD13, we do not believe that the CD90$^+$ cells are adipose-derived stem cells (*60*). Strong CD90 (Thy-1) expression, observed in these cells, is a common marker of most MSCs (*61*) and is indicative of a noncommitted, undifferentiated phenotype (*62*, *63*). Additional studies with more time points will be needed to determine whether these cells begin to differentiate and change their phenotype into other cell types that have been previously identified as residing within the vascular wall, adventitial layers, or perivascular domain (*59*).

Although the temporal and spatial characterization of the host cellular response presented in this study (fig. S11) should facilitate our understanding of clinical HAV remodeling, several limitations of this study must be acknowledged. For example, the results presented on host remodeling only used samples of HAV implanted as an AV conduit for hemodialysis access. Our results may be specific to the anatomical location or physiological conditions of the AV access environment, and HAV implanted in other bypass locations may have different modes of host cell repopulation and remodeling. Of the 60 patients implanted with the HAV in our phase 2 clinical trials, 13 required normal surgical interventions that resulted in explant of a portion of the HAV. Thus, all explanted HAV tissues were obtained because of a need for surgical intervention and from a relatively small sample population (16 different explanted tissues from 13 patients). The influence of weekly cannulations and surgical interventions, such as the previously discussed potential damage to the endothelium during thrombectomies, may have limited our ability to evaluate HAV remodeling under normal unadulterated conditions; however, this was anticipated on the basis of the clinical trial design. Nonetheless, we believe that our results demonstrate that the HAV is recellularized by noninflammatory host progenitor and vascular cells that evolve during time of implantation into mature vascular phenotypes to establish capillary networks and aligned, mature SMC layers. Thus, over time, the resultant HAV becomes like the patients' own self-sustaining blood vessel.

MATERIALS AND METHODS

Study design

This study aimed to provide a spatial and temporal evaluation of host cell repopulation and remodeling of tissue-engineered HAVs implanted as hemodialysis access conduits in humans. Sixteen clinical tissue explants were retrieved 16 to 200 weeks after implantation during clinical interventions from 13 of 60 patients enrolled in two phase 2 clinical trials (table S1). All 16 explanted tissue samples were fixed, processed, and histologically stained for evaluation; four HAV explants were selected for focused in-depth characterization and discussion of results, according to chronological distribution of time after implantation (16, 55, 100, and 200 weeks). Representative staining images from the entire set of 16 HAV explant samples are shown in figs. S1 to S10.

A detailed description of clinical trial design, participant selection, and study monitoring is provided in Lawson *et al.* (*17*). Briefly, 60 patients (aged 18 to 80 years) with ESRD, deemed not suitable for AV fistula creation by the operative surgeon, were enrolled in two single-arm phase 2 clinical studies at six centers in Poland (40 patients) and the United States (20 patients) to receive an HAV implantation for use as an AV graft to provide hemodialysis access. Both the Polish and U.S. studies (clinical trial identifiers NCT01840956 and NCT01744418, respectively) were conducted in accordance with international principles of Good Clinical Practice (ISO14155 and ECH E6/E8/E2A) and the Declaration of Helsinki. The ethics committee or institutional review board of each participating clinical center approved the study protocol, and each patient provided written informed consent before enrollment.

Clinical HAV implantation and follow-up in dialysis patients

The HAVs were implanted in the upper arm (above the elbow) using standard vascular surgical techniques. In 59 patients, the HAVs were placed as a brachial-to-axillary straight graft; in one patient, the HAV was placed in an axillary-to-axillary loop configuration. HAV patency was verified by intraoperative and/or postoperative doppler ultrasound. Aspirin was initiated after surgery (United States) or upon cessation of subcutaneous low molecular weight heparin (Poland) and continued for the duration of follow-up. Follow-up visits occurred at 4 to 7 days (United States only), 15 days, and then monthly until 6 months, followed by visits at 9, 12, 18, and 24 months. At each visit, the HAV and the patient were assessed clinically for signs of infection, adverse responses, and patency (from day 15 onward). Laboratory assessments taken at multiple times during the follow-up period included hematological, clinical chemistry, coagulation analysis, and screening for panel-reactive antibodies and detection of any immunoglobulin G antibodies able to bind to a solubilized unimplanted HAV sample using a custom enzyme-linked immunosorbent assay (*17*). Dialysis cannulation was permitted using the HAV after the 8-week visit (first 30 Polish patients and all U.S. patients) or after the 4-week visit (final 10 Polish patients). Patients continued to use the HAV for dialysis three times a week throughout follow-up.

HAV production and characterization

Bioengineered HAVs 35 to 42 cm long with an inner diameter of 6 mm were generated using production methods previously described (*17*, *19*). Briefly, primary human vascular cells were isolated from cadaveric donor tissue expanded during cell culture and then seeded onto rapidly degradable polyglycolic acid (PGA) tubular scaffolds at a density of 1 million cells/cm. The seeded scaffolds were housed in sterile bioreactors within a perfusion and pump system that delivered pulsatile cyclic distension and media exchange during 8 weeks of incubated tissue culture. During this time, the vascular cells proliferate and secrete ECM proteins, whereas the PGA scaffold degrades. The resulting tubular ECM vessel was then rendered acellular through a decellularization process previously described (*19*) to eliminate cellular antigens but maintain the vessel's protein structure, which is primarily composed of collagen types I and III.

HAVs were characterized for structural and mechanical properties before implantation by measuring suture retention strength, burst pressure, wall thickness, and collagen content (*4*). Analysis of decellularization efficiency confirmed no visible nuclei remained in the acellular vessels after sectioning and staining with H&E, and there were minimal concentrations of residual β-actin protein (59 ng/cm of HAV; $n = 98$ HAV), MHC I (300 pg/cm of HAV; $n = 52$ HAV), and the absence of DNA bands greater than 200 base pairs within homogenized samples analyzed by gel electrophoresis.

Tissue fixation and histological staining

Samples of HAV tissue (unimplanted or clinical explants) were fixed in 10% neutral buffered formalin and embedded into paraffin for sectioning (a thickness of 5 μm) and staining. After deparaffinization and rehydration, H&E and Masson's trichrome staining were performed using standard techniques. StatLab reagents were used for H&E staining, whereas a Masson's trichrome staining kit no. K037 was purchased from Poly Scientific R&D Corporation. Tissue sections of human aorta (American MasterTech CSA0825P) were used as positive controls for H&E and Masson's trichrome staining. Brightfield images were taken using an upright Olympus BX41 microscope equipped with an Olympus DP25 camera and cellSens software.

Immunohistochemistry and fluorescence microscopy

Immunohistochemistry with fluorescence detection was performed using protocols modified from those described by Kajimura *et al.* (*64*). After deparaffinization and rehydration, tissue sections were briefly washed in phosphate-buffered saline with 0.05% Tween 20 (PBST) for 5 min. Heat-induced epitope retrieval was performed in tris EDTA buffer (pH 9.0) containing 0.05% Tween 20 for 20 min at ~95°C, followed by 30 min of cooling at room temperature. Slides were rinsed in distilled water and then twice in PBST. For reduction of autofluorescence, the slides were then incubated in a solution of 0.25% NH_3 and 70% ethanol for 1 hour at room temperature as previously described (*64*). Tissue sections were then blocked for 1 hour at room temperature in PBS containing 10% normal goat serum, 5% bovine serum albumin (BSA), and 0.2% Triton X-100. Primary antibodies (table S2) were diluted in PBST containing 1% BSA and incubated overnight on the tissue sections (~16 hours) at 4°C. After washing the slides in PBST, fluorescence-conjugated secondary antibodies (goat α-mouse Alexa Fluor 488 and goat α-rabbit Alexa Fluor 594, Invitrogen A11001 and A11012, respectively) were diluted 1:400 in PBST containing 1% BSA and incubated on the tissue sections for 1 hour at room temperature. Slides were then washed repeatedly in PBST, followed by incubation at room temperature for 1 hour in a solution of 0.3% Sudan Black B in 70% ethanol to reduce background and lipofuscin-like autofluorescence as described previously (*64*, *65*). Slides were then mounted using Fluoroshield mounting medium (Invitrogen) containing DAPI to counterstain nuclei. Control tissue slides (American MasterTech), secondary antibody only, and nonspecific isotype control primary antibody staining were used to define appropriate antibody concentrations and confirm target specificity. Stained sections were imaged using a Nikon TE300 fluorescence microscope equipped with a Photometrics CoolSNAP HQ2 camera or a Zeiss LSM 780 confocal microscope (UNC Neuroscience Center). Image acquisition, processing, and quantification of cell population were done using μManager (*66*) or Zeiss ZEN and Fiji (*67*) software packages.

Scanning electron microscopy

Samples of unimplanted HAV tissue were sent to the Clemson University Electron Microscopy Laboratory for processing and SEM imaging. Briefly, HAV samples were fixed in a solution of 2.5% glutaraldehyde in 0.2M cacodylate buffer, followed by multiple rinses in distilled water. The fixed samples used for longitudinal and transverse cross sections were then frozen in liquid nitrogen to better preserve tissue morphology during cutting. Secondary fixation of all samples was done using 1% aqueous osmium for 1 hour, followed by multiple rinses in distilled water. Dehydration was performed using a graded ethanol series, and then, after the final incubation in 100% ethanol, the samples were placed in a 1:1 mix of 100% ethanol and hexamethyldisilazane (HDMS) for 15 min to facilitate solution infiltration and sample drying. Samples were then incubated in two changes of HDMS for 15 min, followed by HDMS evaporation. The dehydrated samples were mounted onto SEM stubs, sputter-coated with platinum, and imaged using a Hitachi S-4800 Field Emission Scanning Electron Microscope.

Statistical analysis

Data are shown as means ± SE or SD as noted in the text. After meeting assumptions for normality (Shapiro-Wilk test), the statistical significance of differences between datasets ($P < 0.05$) was evaluated using one-way ANOVA with post hoc Tukey's multiple comparisons test in GraphPad Prism (GraphPad Software Inc.).

SUPPLEMENTARY MATERIALS

www.sciencetranslationalmedicine.org/cgi/content/full/11/485/eaau6934/DC1

Fig. S1. Representative images of all clinical HAV explants stained with H&E.

Fig. S2. Representative images of all clinical HAV explants immunostained for expression of CD3 and CD20.

Fig. S3. Representative images of all clinical HAV explants immunostained for expression of CD206, CD80, and CD68.

Fig. S4. Representative images of all clinical HAV explants immunostained for expression of αSMA and CNN1.

Fig. S5. Representative images of all clinical HAV explants immunostained for expression of CD31 and CD34.

Fig. S6. Representative images of all clinical HAV explants immunostained for expression of αSMA and Nestin.

Fig. S7. Immunofluorescence staining of αSMA and CD31 in 16-week HAV explant.

Fig. S8. $\alpha SMA^+/Nestin^+$ cells participate in HAV self-healing and repair after cannulation injury.

Fig. S9. Representative images of all clinical HAV explants immunostained for expression of αSMA and CD90.

Fig. S10. Additional immunofluorescence characterization of $CD90^+$ cells in 200-week HAV explant.

Fig. S11. Summary diagram illustrating host cell repopulation and maturation within HAV after implantation.

Table S1. Summary of all clinical HAV explants from phase 2 clinical trials.
Table S2. Antibodies used and application conditions.

REFERENCES AND NOTES

1. GBD 2015 Mortality and Causes of Death Collaborators, Global, regional, and national life expectancy, all-cause mortality, and cause-specific mortality for 249 causes of death, 1980-2015: A systematic analysis for the global burden of disease study 2015. *Lancet* **388**, 1459–1544 (2016).
2. P. Bachleda, L. Kalinova, P. Utikal, M. Kolar, K. Hricova, T. Stosova, Infected prosthetic dialysis arteriovenous grafts: A single dialysis center study. *Surg. Infect. (Larchmt.)* **13**, 366–370 (2012).
3. S. Krishnan, A. W. Clowes, Dacron patch infection after carotid endarterectomy: Case report and review of the literature. *Ann. Vasc. Surg.* **20**, 672–677 (2006).
4. S. L. M. Dahl, J. L. Blum, L. E. Niklason, Bioengineered vascular grafts: Can we make them off-the-shelf? *Trends Cardiovasc. Med.* **21**, 83–89 (2011).
5. M. Schneider, C. Stamm, K. G. M. Brockbank, U. A. Stock, M. Seifert, The choice of cryopreservation method affects immune compatibility of human cardiovascular matrices. *Sci. Rep.* **7**, 17027 (2017).
6. T. J. Keane, S. F. Badylak, The host response to allogeneic and xenogeneic biological scaffold materials. *J. Tissue Eng. Regen. Med.* **9**, 504–511 (2015).
7. Z. Mosala Nezhad, A. Poncelet, L. de Kerchove, P. Gianello, C. Fervaille, G. El Khoury, Small intestinal submucosa extracellular matrix (CorMatrix®) in cardiovascular surgery: A systematic review. *Interact. Cardiovasc. Thorac. Surg.* **22**, 839–850 (2016).
8. M. E. Rendal-Vazquez, A. San Luis Verdes, J. Pombo Otero, R. Segura Iglesias, N. Domenech García, C. Andión Nuñez, Anatomopathological and immunohistochemical study of explanted cryopreserved arteries. *Ann. Vasc. Surg.* **26**, 720–728 (2012).
9. J. S. Woo, M. C. Fishbein, B. Reemtsen, Histologic examination of decellularized porcine intestinal submucosa extracellular matrix (CorMatrix) in pediatric congenital heart surgery. *Cardiovasc. Pathol.* **25**, 12–17 (2016).
10. P. R. Vogt, T. Stallmach, U. Niederhäuser, J. Schneider, G. Zünd, M. Lachat, A. Künzli, M. I. Turina, Explanted cryopreserved allografts: A morphological and immunohistochemical comparison between arterial allografts and allograft heart valves from infants and adults1. *Eur. J. Cardiothorac. Surg.* **15**, 639–645; discussion 644-635 (1999).
11. G. T. Kingston, C. R. Darby, I. S. Roberts, The pathology of depopulated bovine ureter xenografts utilized for vascular access in haemodialysis patients. *Histopathology* **55**, 154–160 (2009).
12. E. Benrashid, C. C. McCoy, L. M. Youngwirth, J. Kim, R. J. Manson, J. C. Otto, J. H. Lawson, Tissue engineered vascular grafts: Origins, development, and current strategies for clinical application. *Methods* **99**, 13–19 (2016).
13. N. Hibino, E. McGillicuddy, G. Matsumura, Y. Ichihara, Y. Naito, C. Breuer, T. Shinoka, Late-term results of tissue-engineered vascular grafts in humans. *J. Thorac. Cardiovasc. Surg.* **139**, 431–436.e2 (2010).
14. T. Sugiura, G. Matsumura, S. Miyamoto, H. Miyachi, C. K. Breuer, T. Shinoka, Tissue-engineered vascular grafts in children with congenital heart disease: Intermediate term follow-up. *Semin. Thorac. Cardiovasc. Surg.* **30**, 175–179 (2018).
15. G. Matsumura, N. Hibino, Y. Ikada, H. Kurosawa, T. Shin'oka, Successful application of tissue engineered vascular autografts: Clinical experience. *Biomaterials* **24**, 2303–2308 (2003).
16. M. Olausson, P. B. Patil, V. K. Kuna, P. Chougule, N. Hernandez, K. Methe, C. Kullberg-Lindh, H. Borg, H. Ejnell, S. Sumitran-Holgersson, Transplantation of an allogeneic vein bioengineered with autologous stem cells: A proof-of-concept study. *Lancet* **380**, 230–237 (2012).
17. J. H. Lawson, M. H. Glickman, M. Ilzecki, T. Jakimowicz, A. Jaroszynski, E. K. Peden, A. J. Pilgrim, H. L. Prichard, M. Guziewicz, S. Przywara, J. Szmidt, J. Turek, W. Witkiewicz, N. Zapotoczny, T. Zubilewicz, L. E. Niklason, Bioengineered human acellular vessels for dialysis access in patients with end-stage renal disease: Two phase 2 single-arm trials. *Lancet* **387**, 2026–2034 (2016).
18. T. N. McAllister, M. Maruszewski, S. A. Garrido, W. Wystrychowski, N. Dusserre, A. Marini, K. Zagalski, A. Fiorillo, H. Avila, X. Manglano, J. Antonelli, A. Kocher, M. Zembala, L. Cierpka, L. M. de la Fuente, N. L'Heureux, Effectiveness of haemodialysis access with an autologous tissue-engineered vascular graft: A multicentre cohort study. *Lancet* **373**, 1440–1446 (2009).
19. S. L. Dahl, A. P. Kypson, J. H. Lawson, J. L. Blum, J. T. Strader, Y. Li, R. J. Manson, W. E. Tente, L. DiBernardo, M. T. Hensley, R. Carter, T. P. Williams, H. L. Prichard, M. S. Dey, K. G. Begelman, L. E. Niklason, Readily available tissue-engineered vascular grafts. *Sci. Transl. Med.* **3**, 68ra9 (2011).
20. L. E. Niklason, J. Gao, W. M. Abbott, K. K. Hirschi, S. Houser, R. Marini, R. Langer, Functional arteries grown in vitro. *Science* **284**, 489–493 (1999).
21. R. Saran, B. Robinson, K. C. Abbott, L. Y. Agodoa, P. Albertus, J. Ayanian, R. Balkrishnan, J. Bragg-Gresham, J. Cao, J. L. Chen, E. Cope, S. Dharmarajan, X. Dietrich, A. Eckard, P. W. Eggers, C. Gaber, D. Gillen, D. Gipson, H. Gu, S. M. Hailpern, Y. N. Hall, Y. Han, K. He, H. Hebert, M. Helmuth, W. Herman, M. Heung, D. Hutton, S. J. Jacobsen, N. Ji, Y. Jin, K. Kalantar-Zadeh, A. Kapke, R. Katz, C. P. Kovesdy, V. Kurtz, D. Lavalee, Y. Li, Y. Lu, K. McCullough, M. Z. Molnar, M. Montez-Rath, H. Morgenstern, Q. Mu, P. Mukhopadhyay, B. Nallamothu, D. V. Nguyen, K. C. Norris, A. M. O'Hare, Y. Obi, J. Pearson, R. Pisoni, B. Plattner, F. K. Port, P. Potukuchi, P. Rao, K. Ratkowiak, V. Ravel, D. Ray, C. M. Rhee, D. E. Schaubel, D. T. Selewski, S. Shaw, J. Shi, M. Shieu, J. J. Sim, P. Song, M. Soohoo, D. Steffick, E. Streja, M. K. Tamura, F. Tentori, A. Tilea, L. Tong, M. Turf, D. Wang, M. Wang, K. Woodside, A. Wyncott, X. Xin, W. Zang, L. Zepel, S. Zhang, H. Zho, R. A. Hirth, V. Shahinian, US renal data system 2016 annual data report: Epidemiology of kidney disease in the United States. *Am. J. Kidney Dis.* **69**, A7–A8 (2017).
22. G. Konig, T. N. McAllister, N. Dusserre, S. A. Garrido, C. Iyican, A. Marini, A. Fiorillo, H. Avila, W. Wystrychowski, K. Zagalski, M. Maruszewski, A. L. Jones, L. Cierpka, L. M. de la Fuente, N. L'Heureux, Mechanical properties of completely autologous human tissue engineered blood vessels compared to human saphenous vein and mammary artery. *Biomaterials* **30**, 1542–1550 (2009).
23. N. L'Heureux, N. Dusserre, G. Konig, B. Victor, P. Keire, T. N. Wight, N. A. Chronos, A. E. Kyles, C. R. Gregory, G. Hoyt, R. C. Robbins, T. N. McAllister, Human tissue-engineered blood vessels for adult arterial revascularization. *Nat. Med.* **12**, 361–365 (2006).
24. F. R. Bertani, P. Mozetic, M. Fioramonti, M. Iuliani, G. Ribelli, F. Pantano, D. Santini, G. Tonini, M. Trombetta, L. Businaro, S. Selci, A. Rainer, Classification of M1/M2-polarized human macrophages by label-free hyperspectral reflectance confocal microscopy and multivariate analysis. *Sci. Rep.* **7**, 8965 (2017).
25. F. Raggi, S. Pelassa, D. Pierobon, F. Penco, M. Gattorno, F. Novelli, A. Eva, L. Varesio, M. Giovarelli, M. C. Bosco, Regulation of human macrophage M1–M2 polarization balance by hypoxia and the triggering receptor expressed on myeloid cells-1. *Front. Immunol.* **8**, 1097 (2017).
26. C. I. Civin, T. Trischmann, N. S. Kadan, J. Davis, S. Noga, K. Cohen, B. Duffy, I. Groenewegen, J. Wiley, P. Law, A. Hardwick, F. Oldham, A. Gee, Highly purified CD34-positive cells reconstitute hematopoiesis. *J. Clin. Oncol.* **14**, 2224–2233 (1996).
27. T. Asahara, T. Murohara, A. Sullivan, M. Silver, R. van der Zee, T. Li, B. Witzenbichler, G. Schatteman, J. M. Isner, Isolation of putative progenitor endothelial cells for angiogenesis. *Science* **275**, 964–966 (1997).
28. C. Wiese, A. Rolletschek, G. Kania, P. Blyszczuk, K. V. Tarasov, Y. Tarasova, R. P. Wersto, K. R. Boheler, A. M. Wobus, Nestin expression–a property of multi-lineage progenitor cells? *Cell. Mol. Life Sci.* **61**, 2510–2522 (2004).
29. R. D. Kirkton, H. L. Prichard, M. Santiago-Maysonet, L. E. Niklason, J. H. Lawson, S. L. M. Dahl, Susceptibility of ePTFE vascular grafts and bioengineered human acellular vessels to infection. *J. Surg. Res.* **221**, 143–151 (2018).
30. M. Alawy, W. Tawfick, M. ElKassaby, A. Shalaby, M. Zaki, N. Hynes, S. Sultan, Late Dacron patch inflammatory reaction after carotid endarterectomy. *Eur. J. Vasc. Endovasc. Surg.* **54**, 423–429 (2017).
31. P. Roy-Chaudhury, B. S. Kelly, M. A. Miller, A. Reaves, J. Armstrong, N. Nanayakkara, S. C. Heffelfinger, Venous neointimal hyperplasia in polytetrafluoroethylene dialysis grafts. *Kidney Int.* **59**, 2325–2334 (2001).
32. D. W. Courtman, B. F. Errett, G. J. Wilson, The role of crosslinking in modification of the immune response elicited against xenogenic vascular acellular matrices. *J. Biomed. Mater. Res.* **55**, 576–586 (2001).
33. A. Couvelard, G. Leseche, J.-Y. Scoazec, O. Groussard, Human allograft vein failure: Immunohistochemical arguments supporting the involvement of an immune-mediated mechanism. *Hum. Pathol.* **26**, 1313–1320 (1995).
34. N. Dobrilovic, P. Soukas, I. Sadiq, L. Goldstein, J. Raman, Early complications of biologic extracellular matrix patch after use for femoral artery repair. *J. Vasc. Surg.* **65**, 705–710 (2017).
35. B. Benedetto, G. Lipkowitz, R. Madden, A. Kurbanov, D. Hull, M. Miller, L. Bow, Use of cryopreserved cadaveric vein allograft for hemodialysis access precludes kidney transplantation because of allosensitization. *J. Vasc. Surg.* **34**, 139–142 (2001).
36. J. A. Beamish, P. He, K. Kottke-Marchant, R. E. Marchant, Molecular regulation of contractile smooth muscle cell phenotype: Implications for vascular tissue engineering. *Tissue Eng. Part B Rev.* **16**, 467–491 (2010).
37. B. Strilic, T. Kucera, J. Eglinger, M. R. Hughes, K. M. McNagny, S. Tsukita, E. Dejana, N. Ferrara, E. Lammert, The molecular basis of vascular lumen formation in the developing mouse aorta. *Dev. Cell* **17**, 505–515 (2009).
38. A. M. Müller, M. I. Hermanns, C. Skrzynski, M. Nesslinger, K. M. Müller, C. J. Kirkpatrick, Expression of the endothelial markers PECAM-1, vWf, and CD34 in vivo and in vitro. *Exp. Mol. Pathol.* **72**, 221–229 (2002).
39. N. Ricard, M. Simons, When it is better to regress: Dynamics of vascular pruning. *PLOS Biol.* **13**, e1002148 (2015).
40. T. Pennel, D. Bezuidenhout, J. Koehne, N. H. Davies, P. Zilla, Transmural capillary ingrowth is essential for confluent vascular graft healing. *Acta Biomater.* **65**, 237–247 (2018).
41. T. Pennel, P. Zilla, D. Bezuidenhout, Differentiating transmural from transanastomotic prosthetic graft endothelialization through an isolation loop-graft model. *J. Vasc. Surg.* **58**, 1053–1061 (2013).

42. M. Deutsch, J. Meinhart, P. Zilla, N. Howanietz, M. Gorlitzer, A. Froeschl, A. Stuempflen, D. Bezuidenhout, M. Grabenwoeger, Long-term experience in autologous in vitro endothelialization of infrainguinal ePTFE grafts. *J. Vasc. Surg.* **49**, 352–362 (2009).
43. U. Lendahl, L. B. Zimmerman, R. D. McKay, CNS stem cells express a new class of intermediate filament protein. *Cell* **60**, 585–595 (1990).
44. T. Sejersen, U. Lendahl, Transient expression of the intermediate filament nestin during skeletal muscle development. *J. Cell Sci.* **106** (Pt. 4), 1291–1300 (1993).
45. J. Mokrý, S. Nemecek, Angiogenesis of extra- and intraembryonic blood vessels is associated with expression of nestin in endothelial cells. *Folia Biol.* **44**, 155–161 (1998).
46. K. Tardif, V. Hertig, C. Dumais, L. Villeneuve, L. Perrault, J.-F. Tanguay, A. Calderone, Nestin downregulation in rat vascular smooth muscle cells represents an early marker of vascular disease in experimental type I diabetes. *Cardiovasc. Diabetol.* **13**, 119 (2014).
47. H. Oikawa, K. Hayashi, C. Maesawa, T. Masuda, K. Sobue, Expression profiles of nestin in vascular smooth muscle cells in vivo and in vitro. *Exp. Cell Res.* **316**, 940–950 (2010).
48. S. Suzuki, J. Namiki, S. Shibata, Y. Mastuzaki, H. Okano, The neural stem/progenitor cell marker nestin is expressed in proliferative endothelial cells, but not in mature vasculature. *J. Histochem. Cytochem.* **58**, 721–730 (2010).
49. A. Chabot, M.-A. Meus, P. Naud, V. Hertig, J. Dupuis, L. Villeneuve, N. El Khoury, C. Fiset, S. Nattel, J.-F. Jasmin, A. Calderone, Nestin is a marker of lung remodeling secondary to myocardial infarction and type I diabetes in the rat. *J. Cell. Physiol.* **230**, 170–179 (2015).
50. V. Hertig, K. Tardif, M. A. Meus, N. Duquette, L. Villeneuve, F. Toussaint, J. Ledoux, A. Calderone, Nestin expression is upregulated in the fibrotic rat heart and is localized in collagen-expressing mesenchymal cells and interstitial CD31$^{(+)}$- cells. *PLOS ONE* **12**, e0176147 (2017).
51. J. Lindqvist, E. Torvaldson, J. Gullmets, H. Karvonen, A. Nagy, P. Taimen, J. E. Eriksson, Nestin contributes to skeletal muscle homeostasis and regeneration. *J. Cell Sci.* **130**, 2833–2842 (2017).
52. A. Calderone, Nestin^{+} cells and healing the infarcted heart. *Am. J. Physiol. Heart Circ. Physiol.* **302**, H1–H9 (2012).
53. L. da Silva Meirelles, A. I. Caplan, N. B. Nardi, In search of the in vivo identity of mesenchymal stem cells. *Stem Cells* **26**, 2287–2299 (2008).
54. R. Hass, C. Kasper, S. Böhm, R. Jacobs, Different populations and sources of human mesenchymal stem cells (MSC): A comparison of adult and neonatal tissue-derived MSC. *Cell Commun. Signal* **9**, 12 (2011).
55. M. F. Pittenger, A. M. Mackay, S. C. Beck, R. K. Jaiswal, R. Douglas, J. D. Mosca, M. A. Moorman, D. W. Simonetti, S. Craig, D. R. Marshak, Multilineage potential of adult human mesenchymal stem cells. *Science* **284**, 143–147 (1999).
56. S. Ergün, D. Tilki, D. Klein, Vascular wall as a reservoir for different types of stem and progenitor cells. *Antioxid. Redox Signal.* **15**, 981–995 (2011).
57. W. C. Chen, T. S. Park, I. R. Murray, L. Zimmerlin, L. Lazzari, J. Huard, B. Péault, Cellular kinetics of perivascular MSC precursors. *Stem Cells Int.* **2013**, 983059 (2013).
58. E. Zengin, F. Chalajour, U. M. Gehling, W. D. Ito, H. Treede, H. Lauke, J. Weil, H. Reichenspurner, N. Kilic, S. Ergün, Vascular wall resident progenitor cells: A source for postnatal vasculogenesis. *Development* **133**, 1543–1551 (2006).
59. P. J. Psaltis, A. Harbuzariu, S. Delacroix, E. W. Holroyd, R. D. Simari, Resident vascular progenitor cells—Diverse origins, phenotype, and function. *J. Cardiovasc. Transl. Res.* **4**, 161–176 (2011).
60. A. Mildmay-White, W. Khan, Cell surface markers on adipose-derived stem cells: A systematic review. *Curr. Stem Cell Res. Ther.* **12**, 484–492 (2017).
61. B. Delorme, J. Ringe, N. Gallay, Y. Le Vern, D. Kerboeuf, C. Jorgensen, P. Rosset, L. Sensebé, P. Layrolle, T. Häupl, P. Charbord, Specific plasma membrane protein phenotype of culture-amplified and native human bone marrow mesenchymal stem cells. *Blood* **111**, 2631–2635 (2008).
62. T. T. Sibov, P. Severino, L. C. Marti, L. F. Pavon, D. M. Oliveira, P. R. Tobo, A. H. Campos, A. T. Paes, E. Amaro Jr., L. F. Gamarra, C. A. Moreira-Filho, Mesenchymal stem cells from umbilical cord blood: Parameters for isolation, characterization and adipogenic differentiation. *Cytotechnology* **64**, 511–521 (2012).
63. D. A. Moraes, T. T. Sibov, L. F. Pavon, P. Q. Alvim, R. S. Bonadio, J. R. Da Silva, A. Pic-Taylor, O. A. Toledo, L. C. Marti, R. B. Azevedo, D. M. Oliveira, A reduction in CD90 (THY-1) expression results in increased differentiation of mesenchymal stromal cells. *Stem Cell Res. Ther.* **7**, 97 (2016).
64. J. Kajimura, R. Ito, N. R. Manley, L. P. Hale, Optimization of single- and dual-color immunofluorescence protocols for formalin-fixed, paraffin-embedded archival tissues. *J. Histochem. Cytochem.* **64**, 112–124 (2015).
65. H. J. Romijn, J. F. M. van Uum, I. Breedijk, J. Emmering, I. Radu, C. W. Pool, Double immunolabeling of neuropeptides in the human hypothalamus as analyzed by confocal laser scanning fluorescence microscopy. *J. Histochem. Cytochem.* **47**, 229–235 (2016).
66. A. D. Edelstein, M. A. Tsuchida, N. Amodaj, H. Pinkard, R. D. Vale, N. Stuurman, Advanced methods of microscope control using μManager software. *J. Biol. Methods* **1**, e10 (2014).
67. J. Schindelin, I. Arganda-Carreras, E. Frise, V. Kaynig, M. Longair, T. Pietzsch, S. Preibisch, C. Rueden, S. Saalfeld, B. Schmid, J.-Y. Tinevez, D. J. White, V. Hartenstein, K. Eliceiri, P. Tomancak, A. Cardona, Fiji: An open-source platform for biological-image analysis. *Nat. Methods* **9**, 676–682 (2012).

Acknowledgments: We thank N. Christoforou, S. Gage, and A. Rose for technical insight and helpful discussions. We also acknowledge the surgical and clinical personnel for HAV implantation, collection of data, and explant tissue. We thank G. Wetzel and L. Saraf at Clemson University for providing SEM expertise and M. Itano for assistance with confocal microscopy performed at the UNC Neuroscience Center Microscopy Core Facility, supported, in part, by funding from the NIH-NINDS Neuroscience Center Support Grant P30 NS045892 and the NIH-NICHD Intellectual and Developmental Disabilities Research Center Support Grant U54 D079124. **Funding**: This study was supported by Humacyte Inc. and the NIH (R44 HL118736). **Author contributions**: R.D.K. designed and performed immunostaining experiments and all imaging. M.S.-M. embedded and sectioned all tissues and performed histological staining. J.H.L. conducted and supported clinical work. W.E.T., S.L.M.D., and L.E.N. provided technical guidance. H.L.P. contributed to experimental design, technical guidance, and project oversight. All authors contributed to manuscript writing and revision. **Competing interests**: The authors have relationships with Humacyte Inc., which include board membership, ownership of stock or stock options, employment, and/or consulting agreements. L.E.N. is an inventor on patent 6,537,567 held by MIT that covers tissue-engineered tubular construct having circumferentially oriented SMCs. L.E.N. and S.L.M.D. are inventors on patent 6,962,814 held by Duke University that covers decellularized tissue-engineered constructs and tissues. L.E.N., S.L.M.D., and H.L.P. are inventors on patents 9,556,414 and 9,657,265 held by Humacyte Inc. that cover tissue-engineered constructs and tubular tissue-engineered constructs. H.L.P. is the Chief Operations Officer of Humacyte Inc. H.L.P., R.D.K., W.E.T., M.S.-M., and J.H.L. are all employed by Humacyte Inc. W.E.T. has ownership (stock) in Humacyte Inc. L.E.N. is a founder of Humacyte Inc., has ownership (stock) in Humacyte Inc., receives payments for being a member of the Board of Directors of Humacyte Inc., and receives an unrestricted research grant from Humacyte Inc. **Data and materials availability:** All data associated with this study are present in the paper or the Supplementary Materials.

Submitted 10 July 2018
Accepted 6 March 2019
Published 27 March 2019
10.1126/scitranslmed.aau6934

Citation: R. D. Kirkton, M. Santiago-Maysonet, J. H. Lawson, W. E. Tente, S. L. M. Dahl, L. E. Niklason, H. L. Prichard, Bioengineered human acellular vessels recellularize and evolve into living blood vessels after human implantation. *Sci. Transl. Med.* **11**, eaau6934 (2019).

Science Translational Medicine

Bioengineered human acellular vessels recellularize and evolve into living blood vessels after human implantation

Robert D. Kirkton, Maribel Santiago-Maysonet, Jeffrey H. Lawson, William E. Tente, Shannon L. M. Dahl, Laura E. Niklason and Heather L. Prichard

Sci Transl Med **11**, eaau6934.
DOI: 10.1126/scitranslmed.aau6934

Vital vessels

Vascular access is critically important for hemodialysis. An arteriovenous fistula generated from native blood vessels has long been thought to be optimal for long-term access; however, some people with kidney disease require vascular grafts. Kirkton *et al.* studied bioengineered human acellular vessels (HAVs) implanted as hemodialysis access vessels in subjects with end-stage renal disease. Sixteen tissue samples from HAVs were explanted from subjects participating in phase 2 clinical studies over the course of nearly 4 years. The authors characterized cellular repopulation of the implanted vessels over time, noting increases in $CD90^+$ cells, lumen-lining $CD31^+$ endothelium, and the presence of aligned alpha smooth muscle actin–expressing cells. This study provides valuable insight into human vascular remodeling.

Science Translational Medicine (ISSN 1946-6242) is published by the American Association for the Advancement of Science, 1200 New York Avenue NW, Washington, DC 20005. The title *Science Translational Medicine* is a registered trademark of AAAS.